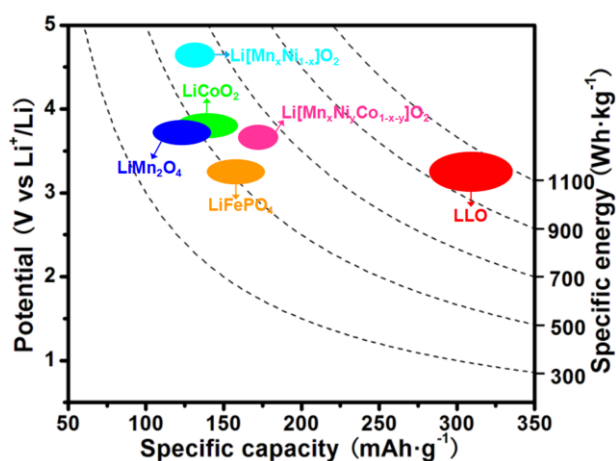


## Supporting Information

# Novel MOF Shell-Derived Surface Modification of Li-Rich Layered Oxide Cathode for Enhanced Lithium Storage

Zhitong Xiao,<sup>1</sup> Jiashen Meng,<sup>1</sup> Qi Li,<sup>1</sup> Xuanpeng Wang,<sup>1</sup> Meng Huang,<sup>1</sup> Ziang Liu,<sup>1</sup> Chunhua Han<sup>1,\*</sup> and Liqiang Mai<sup>1,2,\*</sup>



**Fig. S1** A comparison of reversible capacity and operating voltage ranges of the typical lithium-containing cathode materials. The energy density is calculated on the basis of the voltage versus metallic lithium for simplicity.

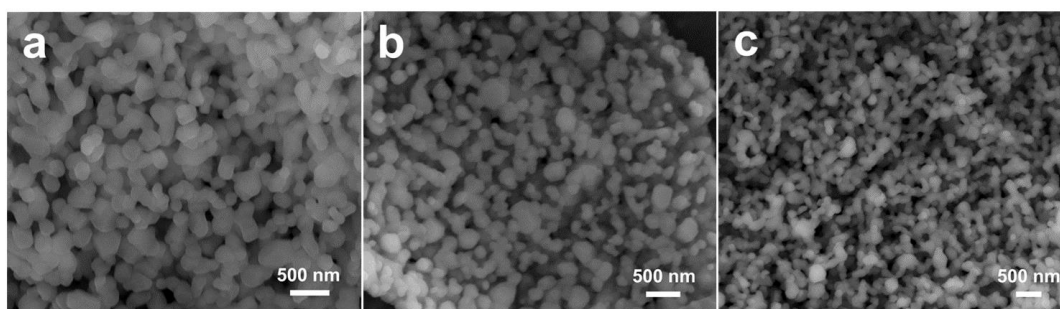


**Fig. S2** (a-c) SEM images of LLO, LLO@MOF and LLO@C&NiCo, respectively.

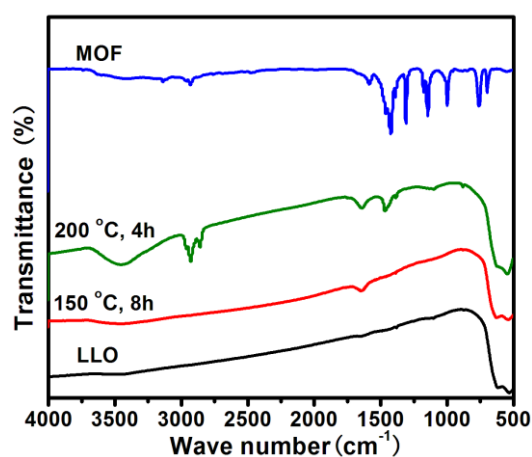


**Fig. S3** FT-IR spectra of LLO, LLO processed by low-pressure vapor superassembly at 150 °C for 8 h, and at 200 °C 4 h, together with a control sample MOF samples.

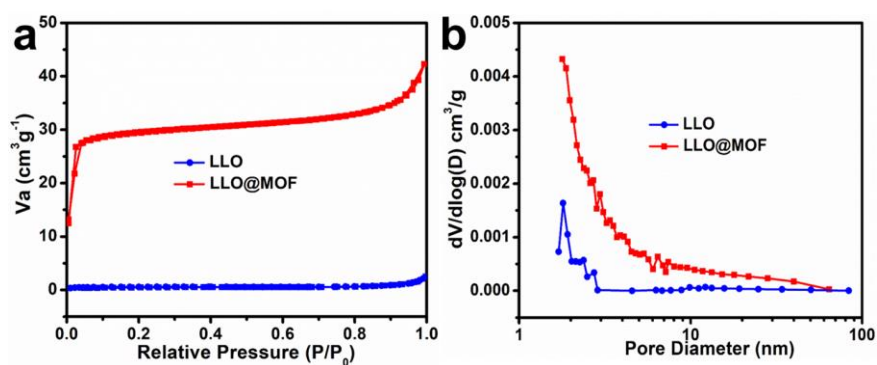


**Fig. S4** (a) N<sub>2</sub> adsorption/desorption isotherm and (b) the corresponding pore size distribution of LLO and LLO@MOF.

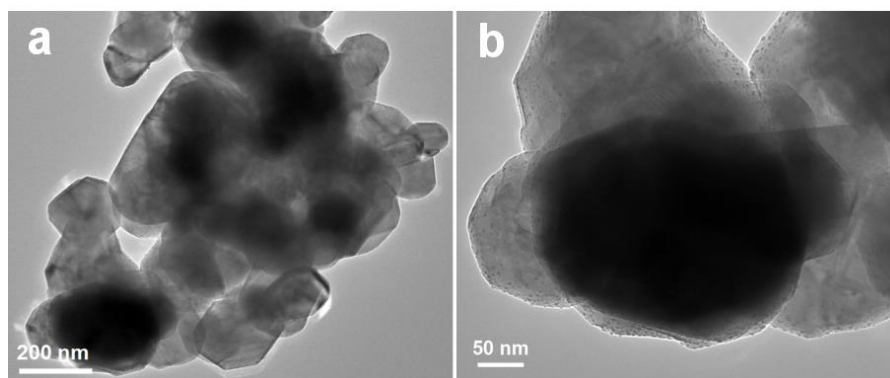


**Fig. S5** TEM images of LLO@C&NiCo.

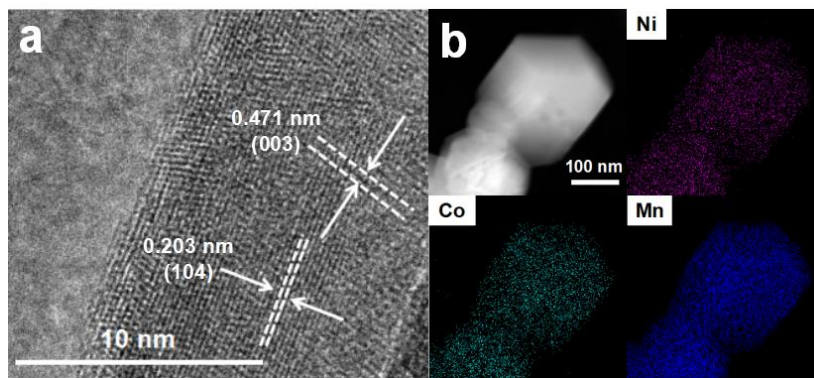


**Fig. S6** (a) HRTEM image and (b) TEM mapping images of LLO.

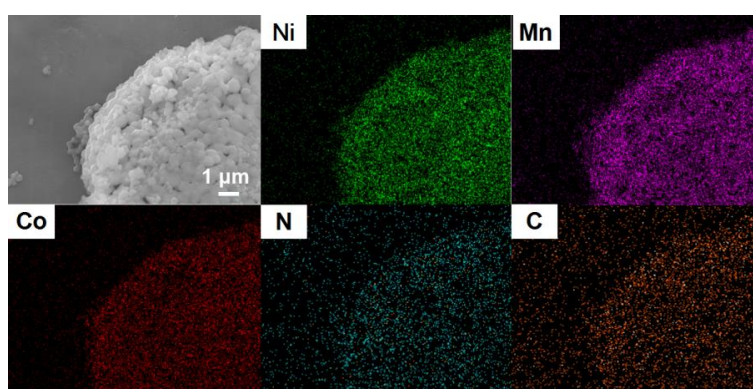


**Fig. S7** SEM elemental mapping images of LLO@C&NiCo.

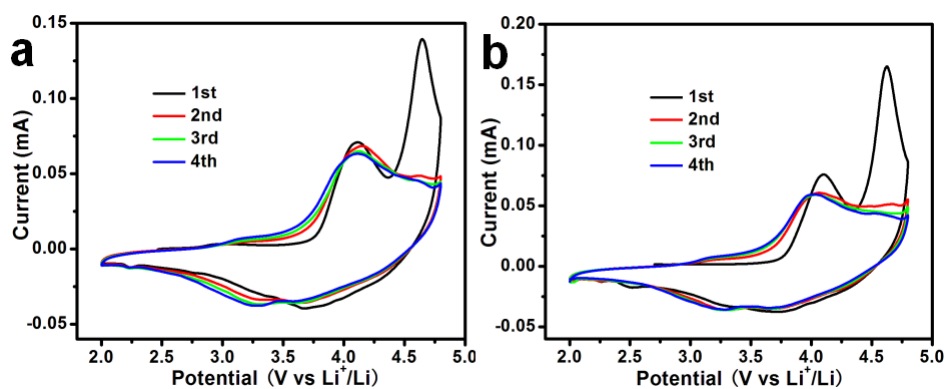


**Fig. S8** CV curves of the first four cycles at the scan rate of  $0.2 \text{ mV s}^{-1}$  of LLO (a) and LLO@C&NiCo (b) in the 2.0-4.8 V range.

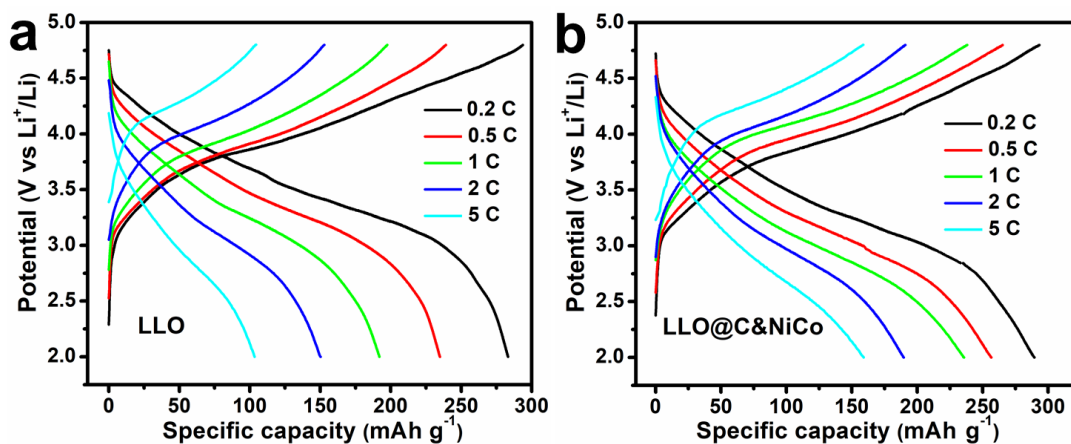


**Fig. S9** The charge-discharge voltage profiles of the LLO (a) and LLO@C&NiCo (b) at different current densities.

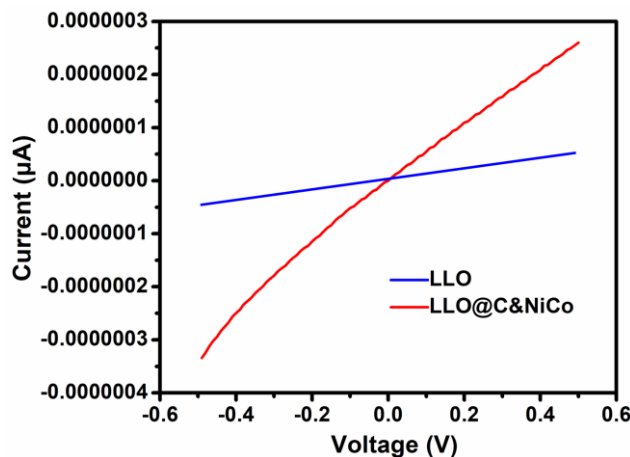


**Fig. S10** I-V curves of LLO and LLO@C&NiCo.

**Table S1.** Electrochemical performance comparison of various modified Li-rich layered oxide cathodes.

Li-rich layered oxide cathode	Voltage range (V)	Current density (mA g <sup>-1</sup> )	Cycle number	Residual		Reference
				capacity (mAh g <sup>-1</sup> )	Capacity retention	
LLO@C&NiCo	2-4.8	100	100	270	95%	Our work
		500	300	178	90%	
Li <sub>1.2</sub> Ni <sub>0.13</sub> Co <sub>0.13</sub> Mn <sub>0.54</sub> O <sub>2</sub> used CMC	2-4.8	200	500	178	79%	S1

binder						
Concentration-gradient PO <sub>4</sub> <sup>3-</sup> polyanion doped LLO	2-4.8	100	400	228.5	88.2%	S2
3D hollow hierarchical structure LLO	2-4.8	125	200	225	89.5%	S3
Fusiform porous micro-nano structure LLO	2-4.6	125	200	256.78	87.1%	S4
Full microwave synthesized LLO	2.5-4.8	200	100	197.2	83.3%	S5
Spherical core-shell structure Li <sub>1.2</sub> Ni <sub>0.2</sub> Mn <sub>0.6</sub> O <sub>2</sub> @Li <sub>1.2</sub> Ni <sub>0.4</sub> Mn <sub>0.4</sub> O <sub>2</sub>	2-4.8	200	100	175	93.1%	S6
Spinel-structure skin and ferric oxide islands coated LLO	2-4.8	250	150	200	80%	S7
0.5 Li <sub>2</sub> MnO <sub>3</sub> 0.5 LiNi <sub>0.8-</sub> Co <sub>0.1</sub> Mn <sub>0.1</sub> O <sub>2</sub> (LL-811) cathode	2-4.7	50	100	195	92%	S8
PEDOT:PSS conducting polymer coated LLO	2-4.8	250	100	146.9	80%	S9
Li <sub>2</sub> ZrO <sub>3</sub> coated LLO	2.5-4.8	250	100	162	83.5%	S10

## References

1. Zhang S, Gu H, Pan H, et al. A novel strategy to suppress capacity and voltage fading of Li-and Mn-rich layered oxide cathode material for lithium-ion batteries. *Adv Energy Mater* 2017; 7:1601066.
2. Hou P, Li G, Gao X. Tailoring atomic distribution in micron-sized and spherical Li-rich layered oxides as cathode materials for advanced lithium-ion batteries. *J Mater Chem A* 2016; 4:7689-7699.
3. Yu F, Que L, Wang Z, et al. Layered-spinel capped nanotube assembled 3D Li-rich architectures for high performance Li-ion battery cathodes. *J Mater Chem A* 2016; 4:18416-18425.

4. Wang G, Wang X, Yi L, et al. Preparation and performance of  $0.5\text{Li}_2\text{MnO}_3 \cdot 0.5\text{LiNi}_{1/3}\text{Co}_{1/3}\text{Mn}_{1/3}\text{O}_2$  with a fusiform porous micro-nano structure. *J Mater Chem A* 2016; 4:15929-15939.
5. Shi S, Zhang S, Wu Z, et al. Full microwave synthesis of advanced Li-rich manganese based cathode material for lithium ion batteries. *J Power Sources* 2017; 337:82-91.
6. Chong S, Wu Y, Chen Y, et al. A strategy of constructing spherical core-shell structure of  $\text{Li}_{1.2}\text{Ni}_{0.2}\text{Mn}_{0.6}\text{O}_2 @ \text{Li}_{1.2}\text{Ni}_{0.4}\text{Mn}_{0.4}\text{O}_2$ , cathode material for high-performance lithium-ion batteries. *J Power Sources* 2017; 356:153-162.
7. Chen S, Zheng Y, Lu Y, et al. Enhanced electrochemical performance of layered lithium-rich cathode materials by constructing spinel-structure skin and ferric oxide islands. *ACS Appl Mater Interfaces* 2017; 9:8669-8678.
8. Shi J, Zhang J, He M, et al. Mitigating voltage decay of Li-rich cathode material via increasing Ni-content for lithium-ion batteries. *ACS Appl Mater Interfaces* 2016; 8:20138-20146.
9. Wu F, Liu J, Li L, et al. Surface modification of Li-rich cathode materials for lithium-ion batteries with a PEDOT:PSS conducting polymer. *ACS Appl Mater Interfaces* 2016; 8:23095-23104.
10. Zhang J, Zhang H, Gao R, et al. New insights into the modification mechanism of Li-rich  $\text{Li}_{1.2}\text{Mn}_{0.6}\text{Ni}_{0.2}\text{O}_2$  coated by  $\text{Li}_2\text{ZrO}_3$ . *Phys Chem Chem Phys* 2016; 18:13322-13331.